

## A 95 GeV Higgs Boson in the Georgi-Machacek Model

Ting-Kuo Chen,<sup>1,\*</sup> Cheng-Wei Chiang,<sup>2,3,†</sup> Sven Heinemeyer,<sup>4,‡</sup> and Georg Weiglein<sup>5,6,§</sup>

<sup>1</sup>*Department of Physics, University of Wisconsin-Madison, Madison, WI 53706, USA*

<sup>2</sup>*Department of Physics and Center for Theoretical Physics,  
National Taiwan University, Taipei, Taiwan 10617, ROC*

<sup>3</sup>*Physics Division, National Center for Theoretical Sciences, Taipei, Taiwan 10617, ROC*

<sup>4</sup>*Instituto de Física Teórica UAM-CSIC, Cantoblanco, 28049, Madrid, Spain*

<sup>5</sup>*Deutsches Elektronen-Synchrotron DESY,  
Notkestr. 85, 22607 Hamburg, Germany*

<sup>6</sup>*II. Institut für Theoretische Physik, Universität Hamburg,  
Luruper Chaussee 149, 22607 Hamburg, Germany*

### Abstract

CMS and ATLAS have reported small excesses in the search for low-mass Higgs bosons in the di-photon decay channel at exactly the same mass, 95.4 GeV. These searches rely on improved analysis techniques, enhancing in particular the discrimination against the  $Z \rightarrow e^+e^-$  background. In models beyond the Standard Model (SM) that extend the Higgs sector with triplets, doubly-charged Higgs bosons are predicted which can contribute substantially to the di-photon decay rate of a light Higgs boson. The Georgi-Machacek (GM) Model is of particular interest in this context, since despite containing Higgs triplets it preserves the electroweak  $\rho$ -parameter to be 1 at the tree level. We show that within the GM model, a Higgs boson with a mass of  $\sim 95$  GeV with a di-photon decay rate as observed by CMS and ATLAS can be well described. We discuss the di-photon excess in conjunction with an excess in the  $b\bar{b}$  final state observed at LEP and an excess observed by CMS in the di-tau final state, which have been found at comparable masses with local significances of about  $2\sigma$  and  $3\sigma$ , respectively. The presence of a Higgs boson at about 95 GeV within the GM model would imply good prospects of the searches for additional light Higgs bosons. In particular, the observed excess in the di-photon channel would be expected to be correlated in the GM model with a light doubly-charged Higgs boson in the mass range between 100 GeV and 200 GeV, which motivates dedicated searches in upcoming LHC Runs.

---

\* [tchen463@wisc.edu](mailto:tchen463@wisc.edu)

† [chengwei@phys.ntu.edu.tw](mailto:chengwei@phys.ntu.edu.tw)

‡ [sven.heinemeyer@cern.ch](mailto:sven.heinemeyer@cern.ch)

§ [georg.weiglein@desy.de](mailto:georg.weiglein@desy.de)

## I. INTRODUCTION

In the year 2012, the ATLAS and CMS collaborations discovered a new scalar particle [1, 2]. Within the current theoretical and experimental uncertainties, the properties of the new particle are consistent with the predictions for the Higgs boson of the Standard Model (SM) with a mass of  $\sim 125$  GeV [3, 4]. However, they are also compatible with many scenarios of physics beyond the SM (BSM). While the minimal scalar sector of the SM contains only one physical Higgs particle, BSM scenarios often give rise to an extended Higgs sector containing additional scalar particles. Accordingly, one of the primary objectives of the current and future LHC runs is the search for additional Higgs bosons, which is of crucial importance for exploring the underlying physics of electroweak symmetry breaking. These additional Higgs bosons can have a mass above, but also below 125 GeV.

Searches for Higgs bosons below 125 GeV have been performed at the LEP [5–7], the Tevatron [8] and the LHC [9–15]. Searches for di-photon resonances at the LHC are particularly intriguing and promising in this context, which is also apparent from the fact that this decay mode, due to its comparably clean final state, constitutes one of the two discovery channels of the Higgs boson at 125 GeV. CMS had performed searches for scalar di-photon resonances at 8 TeV and 13 TeV. Results based on the 8 TeV data and the first year of Run 2 data at 13 TeV, corresponding to an integrated luminosity of  $19.7 \text{ fb}^{-1}$  and  $35.9 \text{ fb}^{-1}$ , respectively, showed a local excess of  $2.8\sigma$  at 95.3 GeV [9, 10]. This excess, being present in both the 8 TeV and the 13 TeV datasets, soon received widespread attention, see e.g. Refs. [16–25].

Subsequently, CMS published the result based on their full Run 2 dataset employing substantially refined analysis techniques. The observed excess for a mass of 95.4 GeV, expressed in terms of a signal strength, is given by [15]

$$\mu_{\gamma\gamma}^{\text{CMS}} = \frac{\sigma^{\text{exp}}(gg \rightarrow \phi \rightarrow \gamma\gamma)}{\sigma^{\text{SM}}(gg \rightarrow H \rightarrow \gamma\gamma)} = 0.33_{-0.12}^{+0.19}. \quad (1)$$

Here  $\sigma^{\text{SM}}$  denotes the cross section for a hypothetical SM Higgs boson at the same mass. Analyses using the result based on the full Run 2 data can be found, e.g., in Refs. [26, 27] (see also Ref. [28] for a review).

More recently, ATLAS presented the result based on their full Run 2 dataset [29, 30] (in the following, we refer to their “model-dependent” analysis, which has a higher discriminating power). The new analysis has a substantially improved sensitivity with respect to their analysis based on the previously reported result utilizing  $80 \text{ fb}^{-1}$  [12]. ATLAS finds an excess with a local significance

of  $1.7\sigma$  at precisely the same mass value as the one that was previously reported by CMS, i.e. at 95.4 GeV. This “di-photon excess” corresponds to a signal strength of

$$\mu_{\gamma\gamma}^{\text{ATLAS}} = \frac{\sigma^{\text{exp}}(gg \rightarrow \phi \rightarrow \gamma\gamma)}{\sigma^{\text{SM}}(gg \rightarrow H \rightarrow \gamma\gamma)} = 0.18_{-0.10}^{+0.10}, \quad (2)$$

see Ref. [31] for details. Neglecting possible correlations, a combined signal strength of

$$\mu_{\gamma\gamma}^{\text{exp}} = \mu_{\gamma\gamma}^{\text{ATLAS+CMS}} = 0.24_{-0.08}^{+0.09} \quad (3)$$

was obtained [31], corresponding to an excess of  $3.1\sigma$  at

$$m_{\phi} \equiv m_{\phi}^{\text{ATLAS+CMS}} = 95.4 \text{ GeV}. \quad (4)$$

The excess in the  $\gamma\gamma$  channel is also of interest in view of the fact that LEP reported a local  $2.3\sigma$  excess in the  $e^+e^- \rightarrow Z\phi(\phi \rightarrow b\bar{b})$  searches [6], which is consistent with a Higgs boson with a mass of 95.4 GeV and a signal strength of [16, 32]

$$\mu_{bb}^{\text{exp}} = 0.117 \pm 0.057. \quad (5)$$

In addition to the di-photon excess, CMS also observed another excess compatible with a mass of 95.4 GeV in the search for  $pp \rightarrow \phi \rightarrow \tau^+\tau^-$  [13]. While this excess is most pronounced at a mass of 100 GeV with a local significance of  $3.1\sigma$ , it is also well compatible with a mass of 95.4 GeV, with a local significance of  $2.6\sigma$ . At 95 GeV, the signal strength is determined to be

$$\mu_{\tau\tau}^{\text{exp}} = 1.2 \pm 0.5. \quad (6)$$

ATLAS has not yet published a search in the di-tau final state covering the mass range around 95 GeV. Concerning the CMS excess in the di-tau channel it should be noted that such a large signal strength is in some tension (depending on the model realization) with experimental bounds from recent searches performed by CMS for the production of a Higgs boson in association with a top-quark pair or in association with a  $Z$  boson, with subsequent decay into tau pairs [33], as well as with the searches performed at LEP for the process  $e^+e^- \rightarrow Z\phi(\phi \rightarrow \tau^+\tau^-)$  [6].

Given that all the excesses discussed above occur at a similar mass, the interesting question arises whether they could all be caused by the production of a single new particle – which, if confirmed by future experiments, would be a first unambiguous sign of BSM physics in the Higgs sector. This triggered activities in the literature regarding possible model interpretations that could account for the various excesses, see, besides the studies mentioned above, e.g., Refs. [34–47].

Many model interpretations discussed in the literature employed extensions of the Two Higgs Doublet Model (2HDM). The main reason was to allow for a suppression of the  $\phi b\bar{b}$  coupling,

enhancing in this way the  $\text{BR}(\phi \rightarrow \gamma\gamma)$ , in order to provide an adequate description of the CMS and ATLAS excesses in this channel. However, there is a second possibility to enhance the di-photon decay rate. Additional charged particles in the loop-mediated decay  $H_1 \rightarrow \gamma\gamma$  can yield a positive contribution to the decay rate and in this way result in a sufficiently strong rate. However, as was found in Ref. [24], a second Higgs doublet, providing an additional singly-charged scalar, is not sufficient to yield a relevant effect on  $\text{BR}(\phi \rightarrow \gamma\gamma)$ .

The above-mentioned situation could be different in models with multiply-charged scalars. For example, doubly-charged Higgs bosons exist in models with Higgs triplet fields and can potentially enhance  $\text{BR}(\phi \rightarrow \gamma\gamma)$ . In view of the constraint arising from the electroweak  $\rho$ -parameter, one is led to the Georgi-Machacek (GM) model [48, 49], which has  $\rho^{\text{tree}} = 1$  by construction. This is realized by imposing a global  $SO(4) \cong SU(2)_L \times SU(2)_R \cong SU(2)_V \times SU(2)_A$  symmetry to the extended Higgs potential. After electroweak symmetry breaking, the custodial  $SU(2)_V$  symmetry is preserved at tree level, and thus contributions to  $\rho$  will only arise at loop levels. The model also has the capability of providing Majorana mass to neutrinos through the lepton number-violating couplings between the complex Higgs triplet and lepton fields. Moreover, it predicts the existence of several Higgs multiplets, whose mass eigenstates form one quintet ( $H_5$ ), one triplet ( $H_3$ ), and two singlets ( $H_1$  and  $h$ ) under the custodial symmetry.

In this paper, we analyze the GM model with respect to the various excesses found around  $\sim 95$  GeV. Previous studies focused on extensions of the GM model [44, 46]. Most recently, while finalizing this manuscript, Ref. [50] appeared, investigating the excesses at  $\sim 95$  GeV in the GM model. In that work, contrary to our analysis (see the detailed discussion below), several Higgs bosons of the GM model are assumed to have masses around  $\sim 95$  GeV, resulting in overlapping signals and leading potentially to somewhat larger rates in the di-tau channel. On the other hand, as will be explained below, our treatment of the various Higgs-boson exclusion bounds and LHC rate measurements includes all relevant data, in particular also from Simplified Template Cross Sections (STXS) measurements. The incorporation of the latest results regarding the measured properties of the detected Higgs boson at  $\sim 125$  GeV as well as of a comprehensive set of the existing limits from additional Higgs searches at the LHC and previous colliders can be particularly relevant for the case of several light Higgs bosons. Furthermore, we include here an analysis of future explorations of the GM interpretation of the  $\sim 95$  GeV excesses.

As will be illustrated below, we identify  $h$  with the discovered Higgs boson at about 125 GeV, and  $H_1$  with the putative Higgs boson state at 95 GeV. Because of mixing among the Higgs doublet and triplet fields, the GM model presents a richer Higgs phenomenology through the couplings of

the SM fermions and gauge bosons with the various Higgs boson states. We will furthermore demonstrate that, as a consequence of the fact that the scale of all the exotic scalar masses (i.e., the masses of all the additional Higgs bosons besides the one at about 125 GeV) are determined by the triplet mass parameter  $m_2^2$  (see Eq. (8) below) and taking into account the theoretical and currently available experimental constraints, the existence of the state  $H_1$  at about 95 GeV implies that all the exotic Higgs bosons have masses at the electroweak scale. We will show that this gives rise to very good prospects for probing this scenario with future results from the LHC experiments<sup>1</sup>.

The paper is organized as follows. After a brief review of the model in Sec. II we list all relevant theoretical and experimental constraints in Sec. III and describe our corresponding analysis flow. The results are presented in Sec. IV, and the future expectations of how such a scenario can be further analyzed at the HL-LHC or a future  $e^+e^-$  collider are discussed in Sec. V. Our conclusions are given in Sec. VI.

## II. THE GEORGI-MACHACEK MODEL

In this section, we give a brief overview of the GM model and introduce our notation. The scalar sector of the GM model comprises one isospin doublet field ( $\phi$ ) with hypercharge  $Y = 1/2$ , one isospin triplet field ( $\chi$ ) with  $Y = 1$ , and one isospin triplet field ( $\xi$ ) with  $Y = 0$ . Under the global  $SU(2)_L \times SU(2)_R$  symmetry that is realized in the GM model, they can be arranged into the following covariant forms

$$\Phi = \begin{pmatrix} (\phi^0)^* & \phi^+ \\ -\phi^- & \phi^0 \end{pmatrix}, \quad \Delta = \begin{pmatrix} (\chi^0)^* & \xi^+ & \chi^{++} \\ -\chi^- & \xi^0 & \chi^+ \\ \chi^{--} & -\xi^- & \chi^0 \end{pmatrix}, \quad (7)$$

where the phase conventions of the charged fields are chosen to be  $(\phi^+)^* = \phi^-$ ,  $(\chi^+)^* = \chi^-$ ,  $(\chi^{++})^* = \chi^{--}$ , and  $(\xi^+)^* = \xi^-$ .

The most general scalar potential consistent with the SM gauge symmetry and the global

---

<sup>1</sup> A  $\mathbb{Z}_2$ -symmetric version of the GM model has been studied in Ref. [51], which may be compatible with  $H_1$  around 95 GeV as well as  $H_3$  and  $H_5$  at the electroweak scale.

$SU(2)_L \times SU(2)_R$  symmetry is given by

$$\begin{aligned}
V(\Phi, \Delta) = & \frac{m_1^2}{2} \text{Tr} [\Phi^\dagger \Phi] + \frac{m_2^2}{2} \text{Tr} [\Delta^\dagger \Delta] + \lambda_1 \left( \text{Tr} [\Phi^\dagger \Phi] \right)^2 + \lambda_2 \left( \text{Tr} [\Delta^\dagger \Delta] \right)^2 \\
& + \lambda_3 \text{Tr} \left[ \left( \Delta^\dagger \Delta \right)^2 \right] + \lambda_4 \text{Tr} [\Phi^\dagger \Phi] \text{Tr} [\Delta^\dagger \Delta] + \lambda_5 \text{Tr} \left[ \Phi^\dagger \frac{\sigma^a}{2} \Phi \frac{\sigma^b}{2} \right] \text{Tr} [\Delta^\dagger T^a \Delta T^b] \quad (8) \\
& + \mu_1 \text{Tr} \left[ \Phi^\dagger \frac{\sigma^a}{2} \Phi \frac{\sigma^b}{2} \right] \left( P^\dagger \Delta P \right)_{ab} + \mu_2 \text{Tr} [\Delta^\dagger T^a \Delta T^b] \left( P^\dagger \Delta P \right)_{ab} ,
\end{aligned}$$

where  $\sigma^a$  and  $T^a$  are the  $2 \times 2$  and  $3 \times 3$  representations of the  $SU(2)$  generators, respectively, and the matrix relating  $\Delta$  to its Cartesian form is given by

$$P = \frac{1}{\sqrt{2}} \begin{pmatrix} -1 & i & 0 \\ 0 & 0 & \sqrt{2} \\ 1 & i & 0 \end{pmatrix} . \quad (9)$$

The neutral fields are parametrized as  $\phi^0 = (v_\Phi + h_\phi + ia_\phi)/\sqrt{2}$ ,  $\chi^0 = (v_\Delta + h_\chi + ia_\chi)/\sqrt{2}$ , and  $\xi^0 = v_\Delta + h_\xi$ , where  $v_\Phi$  and  $v_\Delta$  denote their vacuum expectation values (VEVs). Note that here  $\langle \xi^0 \rangle = \sqrt{2} \langle \chi^0 \rangle$  is required by the imposed global symmetry. The  $SU(2)_L \times SU(2)_R \cong SU(2)_V \times SU(2)_A$  symmetry will be broken spontaneously by the VEVs down to the custodial  $SU(2)_V$  symmetry, with  $v = \sqrt{v_\Phi^2 + 8v_\Delta^2} \simeq 246$  GeV. The two linearly independent minimum conditions are given by

$$\begin{aligned}
m_1^2 = & -4\lambda_1 v_\Phi^2 - 6\lambda_4 v_\Delta^2 - 3\lambda_5 v_\Delta^2 - \frac{3}{2}\mu_1 v_\Delta , \\
m_2^2 = & -12\lambda_2 v_\Delta^2 - 4\lambda_3 v_\Delta^2 - 2\lambda_4 v_\Delta^2 - \lambda_5 v_\Delta^2 - \mu_1 \frac{v_\Phi^2}{4v_\Delta} - 6\mu_2 v_\Delta .
\end{aligned} \quad (10)$$

The scalar fields can be classified according to the isospin values of the custodial  $SU(2)_V$  symmetry into four multiplets:

$$\begin{aligned}
\mathbf{5} : & H_5^{++} = \chi^{++} , H_5^+ = \frac{1}{\sqrt{2}} (\chi^+ - \xi^+) , H_5 = \sqrt{\frac{1}{3}} h_\chi - \sqrt{\frac{2}{3}} h_\xi , \\
\mathbf{3} : & H_3^+ = -\cos \beta \phi^+ + \frac{\sin \beta}{\sqrt{2}} (\chi^+ + \xi^+) , H_3 = \cos \beta a_\phi + \sin \beta a_\chi , \\
\mathbf{1} : & H_1 = \sin \alpha h_\phi + \frac{\cos \alpha}{\sqrt{3}} (\sqrt{2} h_\chi + h_\xi) , \\
\mathbf{1} : & h = \cos \alpha h_\phi - \frac{\sin \alpha}{\sqrt{3}} (\sqrt{2} h_\chi + h_\xi) ,
\end{aligned} \quad (11)$$

where the mixing angle  $\beta$  is defined through  $\tan \beta = v_\phi / (2\sqrt{2}v_\Delta)$ , and the other mixing angle  $\alpha$  through

$$\tan 2\alpha = \frac{2(M^2)_{12}}{(M^2)_{22} - (M^2)_{11}} , \quad \alpha \in \left( -\frac{\pi}{2}, \frac{\pi}{2} \right) , \quad (12)$$

with

$$\begin{aligned}
(M^2)_{11} &= 8\lambda_1 v^2 \sin^2 \beta , \\
(M^2)_{22} &= (3\lambda_2 + \lambda_3)v^2 \cos^2 \beta + M_1^2 \sin^2 \beta - \frac{1}{2}M_2^2 , \\
(M^2)_{12} &= \sqrt{\frac{3}{2}} \sin \beta \cos \beta [(2\lambda_4 + \lambda_5)v^2 - M_1^2] ,
\end{aligned} \tag{13}$$

and

$$M_1^2 = -\frac{v^2}{4v_\Delta} \mu_1, \quad M_2^2 = -12v_\Delta \mu_2 . \tag{14}$$

The tree-level masses of the scalars are then given by

$$\begin{aligned}
m_{H_5}^2 &= m_{H_5^\pm}^2 = m_{H_5^{\pm\pm}}^2 = M_1^2 \frac{v_\Phi^2}{v^2} - \frac{3}{2}\lambda_5 v_\Phi^2 + 8\lambda_3 v_\Delta^2 + M_2^2 , \\
m_{H_3}^2 &= m_{H_3^\pm}^2 = M_1^2 - \frac{1}{2}\lambda_5 v^2 , \\
m_{H_1}^2 &= (M^2)_{11} \sin^2 \alpha + (M^2)_{22} \cos^2 \alpha + 2(M^2)_{12} \sin \alpha \cos \alpha , \\
m_h^2 &= (M^2)_{11} \cos^2 \alpha + (M^2)_{22} \sin^2 \alpha - 2(M^2)_{12} \sin \alpha \cos \alpha .
\end{aligned} \tag{15}$$

In the following, we will identify  $h$  with the detected Higgs boson at about 125 GeV, and  $H_1$  with the possible Higgs boson state at 95 GeV. Accordingly, we set  $m_h = 125$  GeV and  $m_{H_1} = 95$  GeV in the following. In our numerical analysis, the parameter space preferred by the theoretical and experimental constraints that will be discussed below tends to have relatively small  $\alpha$  and  $v_\Delta$  values (see Sec. III). In the limit where  $\alpha, v_\Delta \rightarrow 0$ , known as the decoupling limit, the exotic scalar masses satisfy a decoupling mass relation, and their scale is driven to values far above the electroweak scale [52]. Nevertheless, for the data points passing the applied constraints in our scan, this limit is not exactly realized. Instead, we find that the mass relation mentioned above holds only approximately,

$$2m_{H_1}^2 \approx 3m_{H_3}^2 - m_{H_5}^2 , \tag{16}$$

and that their values can be comparable to the electroweak scale. Since the scale of all the exotic scalar masses is mainly set by the parameter  $m_2^2$  (see Eq. (8)), we expect from both this fact and from the approximate decoupling mass relation of Eq. (16) that the masses  $m_{H_3}$  and  $m_{H_5}$  should also be close to the electroweak scale, which points to the possibility of rich phenomenology with light BSM Higgs bosons. This has also been studied in Ref. [53].

We define the couplings of the SM weak gauge bosons (denoted by  $V$ ) and charged fermions (denoted by  $f$ ) to  $h$  and  $H_1$  in terms of  $\kappa$  factors that modify the couplings as

$$g_{(h,H_1)}(VV,ff) = \kappa_{(h,H_1)}(VV,ff) \times g_{h(VV,ff)}^{\text{SM}} , \tag{17}$$

where in the lowest order

$$\begin{aligned}\kappa_{hVV} &= \sin\beta \cos\alpha - \sqrt{\frac{8}{3}} \cos\beta \sin\alpha, & \kappa_{hff} &= \frac{\cos\alpha}{\sin\beta}, \\ \kappa_{H_1VV} &= \sin\beta \sin\alpha + \sqrt{\frac{8}{3}} \cos\beta \cos\alpha, & \kappa_{H_1ff} &= \frac{\sin\alpha}{\sin\beta}.\end{aligned}\tag{18}$$

We also define for the CP-odd state  $H_3$  and the CP-even state  $H_5$  their respective pseudoscalar and scalar couplings as

$$g_{H_3ff} = \text{sgn}(f) i \cot\beta g_{hff}^{\text{SM}}, \quad g_{H_5VV} = -\frac{\cos\beta}{\sqrt{3}} g_{hVV}^{\text{SM}},\tag{19}$$

where  $\text{sgn}(f = \text{up-type quarks}) = +1$  and  $\text{sgn}(f = \text{down-type quarks, charged leptons}) = -1$ . We note that the  $\mathbf{3}$  multiplet is gauge-phobic, whereas the  $\mathbf{5}$  multiplet is quark-phobic but can couple to leptons if lepton number-violating ( $|\Delta L| = 2$ ) Yukawa couplings are introduced. Also, in the region of relatively small  $\alpha$  and  $v_\Delta$  as described above, we find  $\kappa_{h(VV,ff)} \sim 1$ , as we will show in the numerical analysis in Sec. III, while  $\kappa_{h(VV,ff)} = 1$  holds in the exact decoupling limit.

In our study, we require the scalar potential to satisfy the following three sets of theoretical constraints at tree level:

- **Boundedness-from-below:** The boundedness-from-below constraint can be satisfied as long as the quartic terms of the scalar potential remain positive for all possible field configurations. The sufficient and necessary conditions were first derived in Ref. [54].
- **Perturbative Unitarity:** The perturbative unitarity constraint requires that the zeroth partial-wave mode of all  $2 \rightarrow 2$  scattering channels should be smaller than  $1/2$  at high energies. This was first studied and summarized in Ref. [55].
- **Unique Vacuum:** The unique vacuum constraint requires that the custodially symmetric vacuum should be the unique global minimum in the scalar potential<sup>2</sup>. This can be checked through numerically scanning different combinations of the triplet VEVs  $\langle h_\chi \rangle$  and  $\langle h_\xi \rangle$  [54]. We remark that the assumption of misaligned triplet VEVs would break the custodial  $SU(2)_V$  symmetry down to a  $U(1)$  symmetry, resulting in undesired Goldstone bosons and tachyonic states [58]. A more general scalar potential without the global  $SU(2)_L \times SU(2)_R$  symmetry is required in order to consistently consider the scenario of having misaligned triplet VEVs [59–61].

---

<sup>2</sup> We leave an investigation of the possibility that the custodially symmetric vacuum could be only long-lived rather than being the global minimum within the context of the GM model for future work (see e.g. Refs. [56, 57] for such investigations in the MSSM and the N2HDM).

These constraints are applied to the potential parameters during the sampling process described in Sec. III. For details of the implementation of these theoretical constraints, we refer to Ref. [62].

### III. NUMERICAL ANALYSIS SETUP

#### A. Experimental results for the 95-GeV excess

We quantify the compatibility of the model with the observed excesses at about 95 GeV using

$$\chi_{\gamma\gamma,bb,\tau\tau}^2 = \frac{(\mu_{\gamma\gamma,bb,\tau\tau} - \mu_{\gamma\gamma,bb,\tau\tau}^{\text{exp}})^2}{(\Delta\mu_{\gamma\gamma,bb,\tau\tau}^{\text{exp}})^2}, \quad (20)$$

where the experimental central values and the uncertainties for the observed excesses in the  $\gamma\gamma$ ,  $bb$  and  $\tau\tau$  channels are stated in Sec. I, and  $\mu_{\gamma\gamma,bb,\tau\tau}$  are the theoretically predicted values for the signal strengths in the different channels. Using the framework of coupling modifiers as defined in Eq. (17), the theoretical predictions are given by

$$\mu_{\gamma\gamma} \equiv \mu_{\gamma\gamma,\text{LHC}}^{H_1} \equiv \kappa_{H_1 ff}^2 \times \frac{\text{BR}(H_1 \rightarrow \gamma\gamma)}{\text{BR}(H_1 \rightarrow \gamma\gamma)_{\text{SM}}}, \quad (21)$$

$$\mu_{bb} \equiv \mu_{bb,\text{LEP}}^{H_1} \equiv \kappa_{H_1 VV}^2 \times \frac{\text{BR}(H_1 \rightarrow bb)}{\text{BR}(H_1 \rightarrow bb)_{\text{SM}}}, \quad (22)$$

$$\mu_{\tau\tau} \equiv \mu_{\tau\tau,\text{LHC}}^{H_1} \equiv \kappa_{H_1 ff}^2 \times \frac{\text{BR}(H_1 \rightarrow \tau\tau)}{\text{BR}(H_1 \rightarrow \tau\tau)_{\text{SM}}}, \quad (23)$$

where we assume 100% gluon-fusion production for  $H_1$  at the LHC and denote the branching ratio for a SM-like Higgs boson at 95 GeV to the final state  $X$  as  $\text{BR}(H_1 \rightarrow X)_{\text{SM}}$ . The lowest-order predictions for the coupling modifiers  $\kappa_{H_1 ff}$  and  $\kappa_{H_1 VV}$  are given in Eq. (18).

As mentioned in Sec. I, the di-tau excess observed by CMS at about 95 GeV is in some tension with other searches involving the di-tau final state. On the other hand, the di-photon excess observed by CMS and ATLAS appears to give rise to a more coherent picture. As a consequence, we have chosen to analyze the experimental results at three different levels: 1)  $\gamma\gamma$ , 2)  $\gamma\gamma + bb$ , and 3)  $\gamma\gamma + bb + \tau\tau$ . Thus, we only consider the di-photon excess in the first stage of our two-stage analysis framework (see below), while the question of whether a simultaneous description of the excesses in the  $bb$  and  $\tau\tau$  channels is also possible is investigated in a separate step.

#### B. Parameter scan and point selection

The scalar potential of the GM model contains nine parameters:  $m_{1,2}^2, \lambda_{1,2,3,4,5}, \mu_{1,2}$  (see Eq. (8)). After fixing three of them via the constraints  $m_h = 125$  GeV,  $m_{H_1} = 95$  GeV, and  $v \simeq 246$  GeV,

and trading one more of them with  $v_\Delta$  through one of the minimum conditions (see Eq. (10)), we are left with six independent degrees of freedom. For the numerical analysis, we choose the input parameters to be

$$\{v_\Delta, \lambda_2, \lambda_3, \lambda_5, \mu_1, \mu_2\},$$

and scan them uniformly within the range  $v_\Delta \in [0, 50]$  GeV,  $\lambda_{2,3,5} \in [-4\pi, 4\pi]$ ,  $\mu_1 \in [-500, 0]$  GeV, and  $\mu_2 \in [-500, 500]$  GeV. We perform our numerical analysis in a two-stage framework. The first stage is to use the Bayesian-based Markov-Chain Monte Carlo simulation package `HEPfit` [63] to generate a collection of samples that are “shaped” by the applied theoretical and experimental constraints. The second stage is to further constrain the allowed parameter space by applying the package `HiggsTools` [64] in order to ensure that the allowed parameter regions are in accordance with the measured properties of the detected Higgs boson at 125 GeV (sub-package `HiggsSignals` [64–67], data set v1.1) and with the limits from searches for additional Higgs bosons at the LHC and at LEP (sub-package `HiggsBounds` [64, 68–71], data set v1.2). The employed versions of `HiggsSignals` and `HiggsBounds` include essentially all relevant datasets from the LHC Run 2.

In the first stage, after generating each sample from the previously defined scanning ranges, we calculate the quantities needed to test the theoretical constraints summarized in Sec. II as well as the total likelihood associated with all of the experimental measurements that we take into account at this stage, which include the 95-GeV di-photon excess, the 125-GeV Higgs rate measurements from LHC Run-1, and the  $\text{BR}(b \rightarrow s\gamma)$  measurement [72] (following the methodology of `GM CALC` [73]). All of the samples are then required to satisfy the theoretical constraints and to fall within the 95% Bayesian confidence interval<sup>3</sup>. The reason that we only consider the 125-GeV Higgs rate measurements from LHC Run-1 at this stage is as follows. In both `HEPfit` and `HiggsTools`, the Run-1 measurements are all implemented in terms of signal strengths, i.e. as combinations of production and decay channels. Starting from Run-2, some of the measurements have been presented in terms of the STXS framework, which `HiggsTools` adopts (where `HiggsSignals` ensures that no double counting of measurements occurs<sup>4</sup>), while `HEPfit` still uses

<sup>3</sup> The  $X\%$  (Bayesian) confidence interval is defined as follows. For a collection of samples that are individually assigned with a posterior probability, we sum up all these probabilities and sort the samples in the order of descending probability. Then, starting from the first sample, the serial sub-collection of samples whose probability sum corresponds to  $X\%$  of the overall probability sum is considered to be within the “ $X\%$  confidence interval”.

<sup>4</sup> The code `HiggsSignals` makes use of the LHC measurements for the 125-GeV Higgs boson in the detected final states. These include the combined Run 1 rate [74] measurements, the Run 2 measurements in the following final states,  $WW$  [75–77],  $ZZ$  [78, 79],  $b\bar{b}$  [80–83],  $c\bar{c}$  [84, 85],  $\tau^+\tau^-$  [86–89],  $\mu^+\mu^-$  [90, 91],  $\gamma\gamma$  [92–94], as well as those measured in the  $t\bar{t}H$  production channel [95–97]. Out of these the  $\tau^+\tau^-$  and  $\gamma\gamma$  final states are incorporated via their respective STXS measurements, while for the others the measured signal strengths are implemented.

the same framework as in Run-1. In order to apply the measurements consistently and since an exclusion of certain regions of the parameter space is only carried out in the second stage, we do not consider the Run-2 measurements at the first stage. This is also why we do not apply the limits from searches for additional Higgs bosons at this stage, which is to be considered in the next stage.

In the second stage, we further analyze the samples obtained in the previous stage, including the steps of: 1) rejecting samples that violate the 95% confidence level (CL) limits from experimental searches for additional Higgs bosons using `HiggsBounds` [64, 68–71], and 2) calculating the total  $\chi^2$  of the LHC rate measurements of the observed Higgs boson at 125 GeV, which we denote as  $\chi_{125}^2(\text{GM})$ , for the remaining samples using `HiggsSignals` [64–67]. To evaluate the samples in more detail, we further calculate some additional quantities that are used in the later analysis. Including  $\chi_{125}^2(\text{GM})$ , they are:

- $\chi_{125}^2(\text{GM})$ : The  $\chi^2$  value associated with the rate measurements of the 125-GeV Higgs boson for the individual data points.
- $\chi_X^2(\text{GM})$ : The  $\chi^2$  value associated with the 95-GeV excesses in the  $X = \gamma\gamma, \gamma\gamma + bb, \gamma\gamma + bb + \tau\tau$  channel(s) for the individual data points. For the details, please see the discussion in Secs. I and III A.
- $\chi_{125}^2(\text{SM})$ : The  $\chi^2$  value associated with the rate measurements of the 125-GeV Higgs boson for the case of the SM prediction. We find  $\chi_{125}^2(\text{SM}) \approx 152.5$ .
- $\chi_X^2(\text{SM})$ : The  $\chi^2$  value associated with the 95-GeV excesses in the  $X = \gamma\gamma, \gamma\gamma + bb, \gamma\gamma + bb + \tau\tau$  channel(s) for the case of the SM. We find  $\chi_{\gamma\gamma}^2(\text{SM}) \approx 9.0$ ,  $\chi_{\gamma\gamma+bb}^2(\text{SM}) \approx 13.2$ , and  $\chi_{\gamma\gamma+bb+\tau\tau}^2(\text{SM}) \approx 19.0$ .
- $\Delta\chi_{125}^2$ : The difference in the  $\chi^2$  values associated with the rate measurements of the 125-GeV Higgs boson between the GM model and the SM, given by  $\Delta\chi_{125}^2 \equiv \chi_{125}^2(\text{GM}) - \chi_{125}^2(\text{SM})$ .
- $\Delta\chi_X^2$ :  $\Delta\chi_X^2 \equiv \Delta\chi_{125}^2 + \chi_X^2(\text{GM}) - \chi_X^2(\text{SM})$ .

For each choice of  $X$ , we first select the subset of samples that satisfy  $\Delta\chi_X^2 < 0$ . For such samples, the combined  $\chi^2$  arising from the excess at 95 GeV and the measurements of the Higgs boson at 125 GeV is lower than for the SM. We then further pick from this subset the samples with  $\Delta\chi_{125}^2 < 6.18$ . Such samples fall within the 95.4% (or 2-sigma) CL of the SM prediction for the

125-GeV Higgs measurements for a two-dimensional parameter distribution. Finally, we identify the best-fit points from the latter subsets.

#### IV. NUMERICAL ANALYSIS OF THE 95 GEV HIGGS BOSON

We first present in FIG. 1 the sample distributions in the  $\mu_{H_1}^{\gamma\gamma}-\mu_{H_1}^{bb}$  (left column) and  $\mu_{H_1}^{\gamma\gamma}-\mu_{H_1}^{\tau\tau}$  planes (right column) for three cases: (i)  $X = \gamma\gamma$  (upper row), (ii)  $\gamma\gamma + bb$  (middle row) and (iii)  $\gamma\gamma + bb + \tau\tau$  (lower row). In all plots, we show the (black dashed) 1-sigma ellipses of the respective 95-GeV excesses. The red points fulfill  $\Delta\chi_X^2 < 0$  and  $\Delta\chi_{125}^2 < 6.18$ . They are a subset of the blue points that fulfill  $\Delta\chi_X^2 < 0$ . The best-fit sample is marked by a green star. One can see that in all three cases, the GM model cannot accommodate the  $\tau\tau$  excess. However, a large set of samples can be found within the 1-sigma contour of the  $\mu_{H_1}^{\gamma\gamma}-\mu_{H_1}^{bb}$  plane. It can also be seen that the  $bb$  excess constraint restricts the data to about the left half of the  $\gamma\gamma$  interval while still covering the central value.

We also point out that for the first case, the best-fit point is located well inside the  $1-\sigma$  contour, while for cases (ii) and (iii) it is located right at the boundary and, in particular, at lower  $\mu_{\gamma\gamma}$  values. In view of the fact that the experimental situation regarding the  $\tau\tau$  excess is somewhat unclear (see the discussion in Secs. I and III A), we will present only the results based upon the samples of case (i) in our further study.

A summary of the physical properties of the best-fit point for  $X = \gamma\gamma$  is given in TABLE. I. While this is only an example of one benchmark point, it gives an idea about phenomenologically preferred parameters and decay channels around that region of the parameter space. One can observe that  $\alpha = 0.224$  and  $v_\Delta = 5.24$  GeV (thus  $\cos\beta \approx 0.06$ ), while the values  $m_{H_3} = 105$  GeV and  $m_{H_5} = 121$  GeV show that the mass spectrum of the scalar states lies far below the TeV scale and that the approximate decoupling mass relation  $3m_{H_3}^2 - m_{H_5}^2 \approx 2(95 \text{ GeV})^2$  (see Eq. (16)) is satisfied. These characteristics demonstrate that the preferred parameter space tends to yield  $\kappa_{h(VV,ff)} \approx 1$ , which for the best-fit point have the values  $\kappa_{hVV} = 0.952$ ,  $\kappa_{hff} = 0.977$ . Given the masses of the exotic scalars, the decay of  $H_3$  is dominated by the  $bb$  channel and that of  $H_3^\pm$  by the  $\tau\nu_\tau$  channel. Though the  $H_5$  boson primarily decays into the  $WW$  final state, the branching ratios of the  $\gamma\gamma$  and  $ZZ$  channels are also of the same order. As we will show later, the preferred mass range of  $H_5$  in our samples actually covers the three regimes of  $m_{H_5} \lesssim 2m_W$ ,  $2m_W \lesssim m_{H_5} \lesssim 2m_Z$ , and  $2m_Z \lesssim m_{H_5}$ , thus resulting in a diverse combination of  $\gamma\gamma, WW, ZZ$  channel preferences. However, the production cross sections for  $H_5$  obtained from our samples are all  $\lesssim \mathcal{O}(1 \text{ fb})$ , which

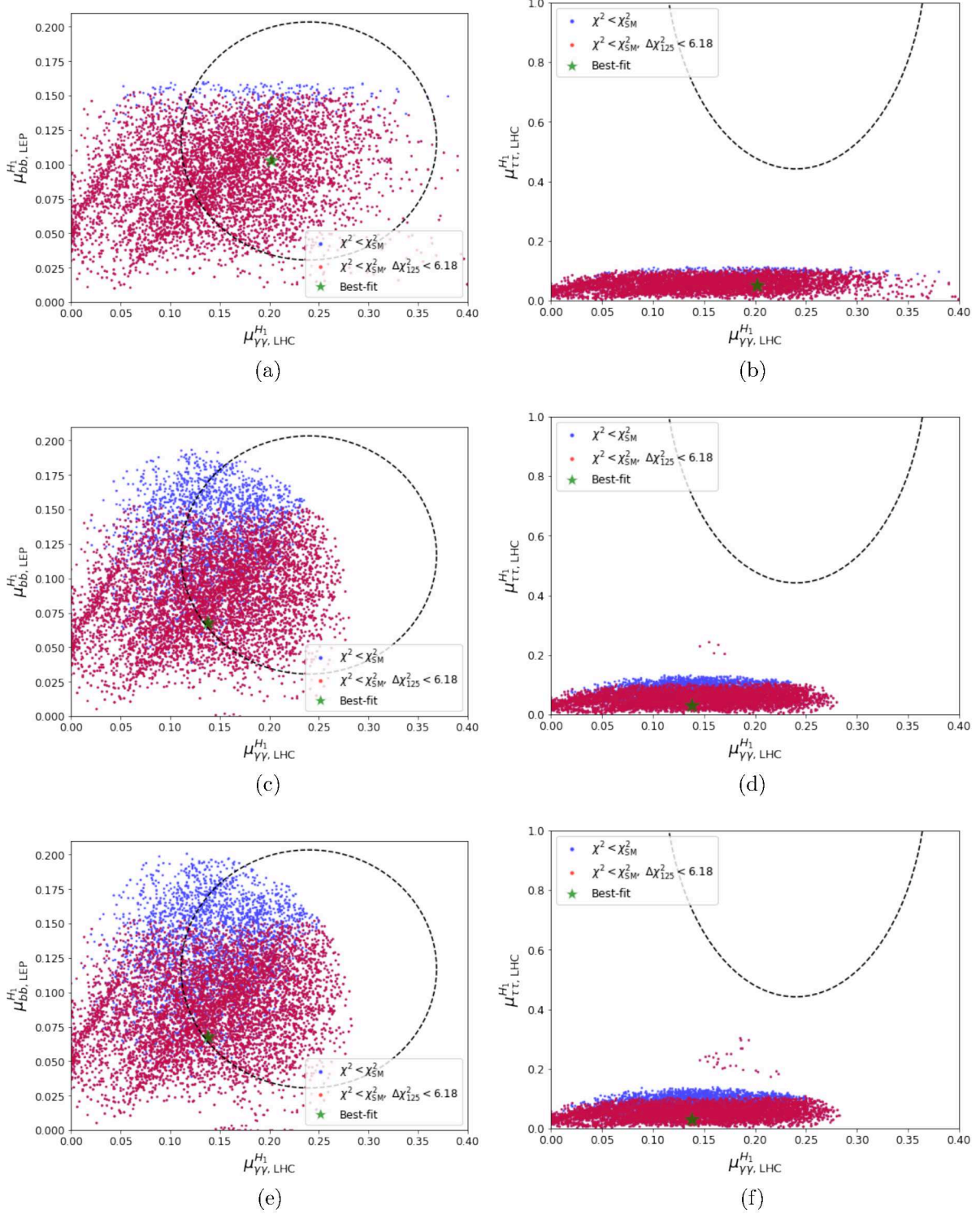


FIG. 1. Sample distributions in the  $\mu_{H_1}^{\gamma\gamma} - \mu_{H_1}^{bb}$  plane for (a)  $X = \gamma\gamma$  (case (i)), (c)  $X = \gamma\gamma + bb$  (case (ii)), and (e)  $X = \gamma\gamma + bb + \tau\tau$  (case (iii)), as well as in the  $\mu_{H_1}^{\gamma\gamma} - \mu_{H_1}^{\tau\tau}$  plane for (b) case (i), (d) case (ii), and (f) case (iii). The elliptic contours denote the 1- $\sigma$  bounds of the corresponding 95-GeV excess measurements.

Best-fit Point Properties		
$\alpha = 0.224, v_\Delta = 5.24 \text{ GeV}, m_{H_3} = 105 \text{ GeV}, m_{H_5} = 121 \text{ GeV}$		
$\kappa_{hVV} = 0.952, \kappa_{hff} = 0.977, \kappa_{H_1VV} = 0.317, \kappa_{H_1ff} = 0.222$		
$\mu_{XX}^{H_1}$	$\gamma\gamma, \text{LHC}$	0.202
	$bb, \text{LEP}$	0.103
	$\tau\tau, \text{LHC}$	0.050
$\text{BR}(h \rightarrow XX)$	$bb$	0.581
	$cc$	0.029
	$\tau\tau$	0.062
	$gg$	0.094
	$\gamma\gamma$	0.002
	$Z\gamma$	0.002
	$ZZ$	0.025
	$WW$	0.204
$\text{BR}(H_1 \rightarrow XX)$	$bb$	0.823
	$cc$	0.041
	$\tau\tau$	0.084
	$gg$	0.034
	$\gamma\gamma$	0.006
	$ZZ$	0.001
	$WW$	0.010
$\text{BR}(H_3 \rightarrow XX)$	$bb$	0.781
	$cc$	0.039
	$\tau\tau$	0.081
	$gg$	0.098
$\text{BR}(H_5 \rightarrow XX)$	$WW$	0.546
	$ZZ$	0.208
	$\gamma\gamma$	0.225
	$Z\gamma$	0.021
$\text{BR}(H_3^\pm \rightarrow \tau\nu_\tau)$	1.0	Off-shell scalar final states are neglected.
$\text{BR}(H_5^\pm \rightarrow WZ)$	1.0	
$\text{BR}(H_5^{\pm\pm} \rightarrow WW)$	1.0	

TABLE I. Summary of the physical properties of the best-fit point in the  $X = \gamma\gamma$  selection.

limits the prospects for probing this state at the LHC in the near future. Finally, though we do not consider their off-shell decays to other scalar states,  $H_5^\pm$  and  $H_5^{\pm\pm}$  primarily decay into  $WZ$  and same-sign  $WW$  final states, respectively, which are the striking signatures of these GM scalar states.

In FIG. 2 we present the sample distributions in the  $\alpha$ - $v_\Delta$  and  $m_{H_3}$ - $m_{H_5}$  planes. In FIG. 2(a), we also plot the contours of  $\kappa_{(h,H_1)(VV,ff)}$ : the solid (dashed) lines denote the  $\kappa_{XVV}$  ( $\kappa_{Xff}$ ) contours for  $X = h$  and  $X = H_1$  in black and purple, respectively. In FIG. 2(b), we also indicate the contour of the approximate decoupling mass relation given by Eq. (16) using a black dashed curve. In contrast to the case of  $m_{H_1} > m_h$ , where one finds  $\alpha < 0$  (see, e.g., Ref. [62]), in our analysis with  $95 \text{ GeV} = m_{H_1} < m_h = 125 \text{ GeV}$ , all the data points are found to have  $\alpha > 0$ . Furthermore, one can see that  $\alpha \lesssim 0.35$  and  $v_\Delta \lesssim 6 \text{ GeV}$ , and thus the magnitudes of the  $\kappa$  values manifest the following features of the small  $\alpha$  and  $v_\Delta$  limit: the  $\kappa_{h(VV,ff)}$  values are close to the SM predictions while  $\kappa_{H_1(VV,ff)} \lesssim 0.4$ . These are further confirmed by plot (b), where all points are found to be very close to the contour indicating the decoupling mass relation given by Eq. (16) in the exact limit. The feature that the preferred parameter region yields  $\kappa_{h(VV,ff)}$  values that are close to the SM predictions can be understood from the fact that all the current measurements of the properties of the Higgs boson at 125 GeV are very consistent with the SM predictions, thus leaving little space for the model parameters to deviate from this limit. Nevertheless, in the GM model the additional triplet gauge couplings provide more flexibility (parametrized by  $\beta$ ) in comparison to the case of just a singlet scalar mixing (parametrized by  $\alpha$ ) to account for both the 125- and 95-GeV Higgs measurements, while also allowing rich phenomenology in the other sectors of the model. Moreover, the smallness of  $m_{H_3}$  and  $m_{H_5}$  ( $\lesssim 160$  and  $230 \text{ GeV}$ , respectively), which is expected from the approximate decoupling mass relation of Eq. (16) and the general scale set by  $m_2^2$  as discussed in Sec. II, suggests that in the GM model the confirmation of the observed excess at about 95 GeV would give rise to exciting prospects regarding possible discoveries of further sub-TeV Higgs bosons at the (HL-)LHC (see the discussion below). As alluded to before, the preferred  $m_{H_5}$  range of  $[90, 230] \text{ GeV}$  covers both the  $2m_W$  and  $2m_Z$  thresholds and thus gives rise to various  $H_5$  decay patterns, but the smallness of its production cross section renders it difficult to be probed in the near future experiments.

In the final step of our analysis of the present experimental situation, we investigate the origin of the relatively large  $\text{BR}(H_1 \rightarrow \gamma\gamma)$ , as required to fit the CMS and ATLAS excesses. Here the  $H_5^{\pm\pm}$ -loop diagram contribution to the effective  $H_1\gamma\gamma$  coupling plays an important role. To study this, we define  $\tilde{\mu}_{\gamma\gamma}^{H_1}$  to be the 95-GeV di-photon signal strength predicted by the GM model

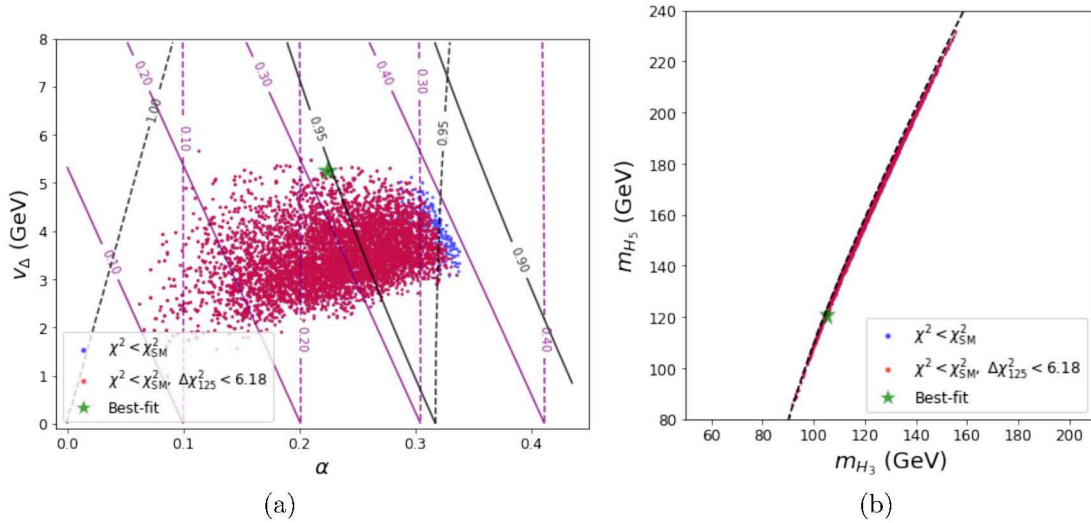


FIG. 2. Sample distributions in the (a)  $\alpha$ - $v_\Delta$  and the (b)  $m_{H_3}$ - $m_{H_5}$  planes for case (i). In plot (a), the solid (dashed) lines denote the  $\kappa_{XVV}$  ( $\kappa_{Xff}$ ) contours for  $X = h$  and  $X = H_1$  in black and purple, respectively. In plot (b), the dashed curve denotes the contour of the coupling mass relation given by Eq. (16) in the exact limit.

“without the  $H_5^{\pm\pm}$ -loop contribution”. The comparison of the results with and without the loop contribution involving  $H_5^{\pm\pm}$  is shown in FIG. 3, where we plot the sample distributions in both the  $m_{H_5}$ - $\mu_{\gamma\gamma}^{H_1}$  and  $m_{H_5}$ - $\tilde{\mu}_{\gamma\gamma}^{H_1}$  planes. One can clearly see that removing the  $H_5^{\pm\pm}$ -loop diagram significantly lowers the 95-GeV di-photon signal strength predictions. This applies especially to points with relatively low  $m_{H_5}$ , as the doubly-charged Higgs boson loop contribution is larger for lighter  $H_5^{\pm\pm}$ . This feature of the GM model (and some other triplet extensions such as the Type-II seesaw model [98–101]) thus motivates the search for a relatively light doubly-charged scalar boson in future experiments. One such search was performed by ATLAS within the context of the GM model [102], which reported a  $2.5\sigma$  excess of  $H_5^{\pm\pm}$  at 450 GeV in the VBF production channel. While this is far above the preferred  $m_{H_5}$  range of our present study, it motivates further dedicated searches for doubly-charged Higgs bosons also for smaller masses at the LHC in the future.

## V. FUTURE PROSPECTS

We finish our analysis by investigating the prospects for testing the GM interpretation of the excesses at 95 GeV. We start with an analysis of the most promising search channels at the HL-LHC in FIG. 4. The upper left plot shows our sample with all points fulfilling  $\chi^2 < \chi_{SM}^2$  and

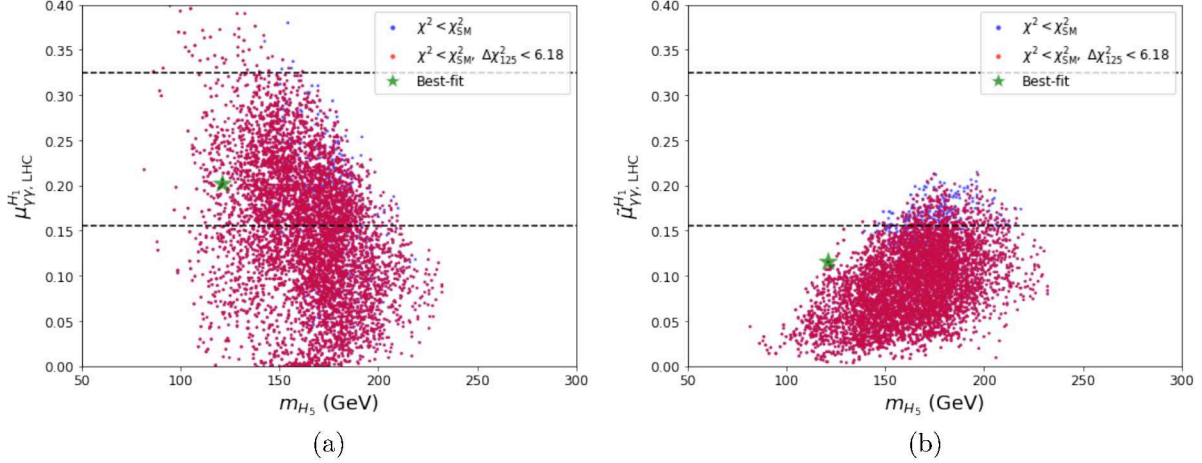


FIG. 3. Sample distributions in the (a)  $m_{H_5} - \mu_{\gamma\gamma}^{H_1}$  and (b)  $m_{H_5} - \tilde{\mu}_{\gamma\gamma}^{H_1}$  planes for case (i).

$\Delta\chi_{125}^2 < 6.18$  in the plane  $m_{H_3} - \sigma(gg \rightarrow H_3 \rightarrow \tau\tau)$ <sup>5</sup>, where the black dashed line indicates the anticipated 95% CL HL-LHC search limit for the search of Higgs bosons decaying to  $\tau^+\tau^-$  [105]. It can be seen that according to the current projections for the achievable sensitivity, it will not be possible to discover  $H_3$  in the  $\tau^+\tau^-$  decay channel. Only with a substantially improved sensitivity will this channel become accessible as a discovery mode at the HL-LHC. The upper right and the lower plot show our sample points in the  $m_{H_5} - \sigma(WZ \rightarrow H_5^\pm \rightarrow WZ)$  and  $m_{H_5} - \sigma(WW \rightarrow H_5^{\pm\pm} \rightarrow WW)$  planes, respectively. No evaluation of the HL-LHC reach is available for these search channels. However, with masses around and not too far below the  $WZ$  and  $WW$  mass shells and cross sections above 1 fb, it may be possible to cover part of the parameter space at the HL-LHC.

Before moving on, we comment on two types of  $H_5^{\pm\pm}$  searches that turn out to impose no or incomplete constraints on the  $m_{H_5}$  range in our samples. The first type of searches are the ones for the process  $H_5^{\pm\pm} \rightarrow \ell^\pm\ell^\pm$ . In the GM model, this process is realized through the lepton number-violating coupling between the  $\chi$  and lepton fields. However, Ref. [52] shows that only for  $v_\Delta \lesssim 10^{-4}$  GeV would this decay channel become comparable to the weak gauge boson decay channels, and thus it is irrelevant for the preferred parameter space of our study. One such search has been performed at LEP, targeting the pair production of  $H_5^{\pm\pm}$  [108]. The second type of searches are the ones for  $H_5^{\pm\pm}$  relying on the decay to two on-shell like-sign  $W$  bosons, which have been performed at the LHC and resulted in a stringent bound of  $m_{H_5} \geq 200$  GeV [109–112]. Therefore, it remains an open question to which extent a doubly-charged Higgs boson  $H_5^{\pm\pm}$  with a

<sup>5</sup> The cross sections used in this section are all obtained from the predictions reported by the LHC Higgs Cross Section Working Group [103, 104], using the  $\kappa$  parameters as specified in Sec. II as coupling modifiers.

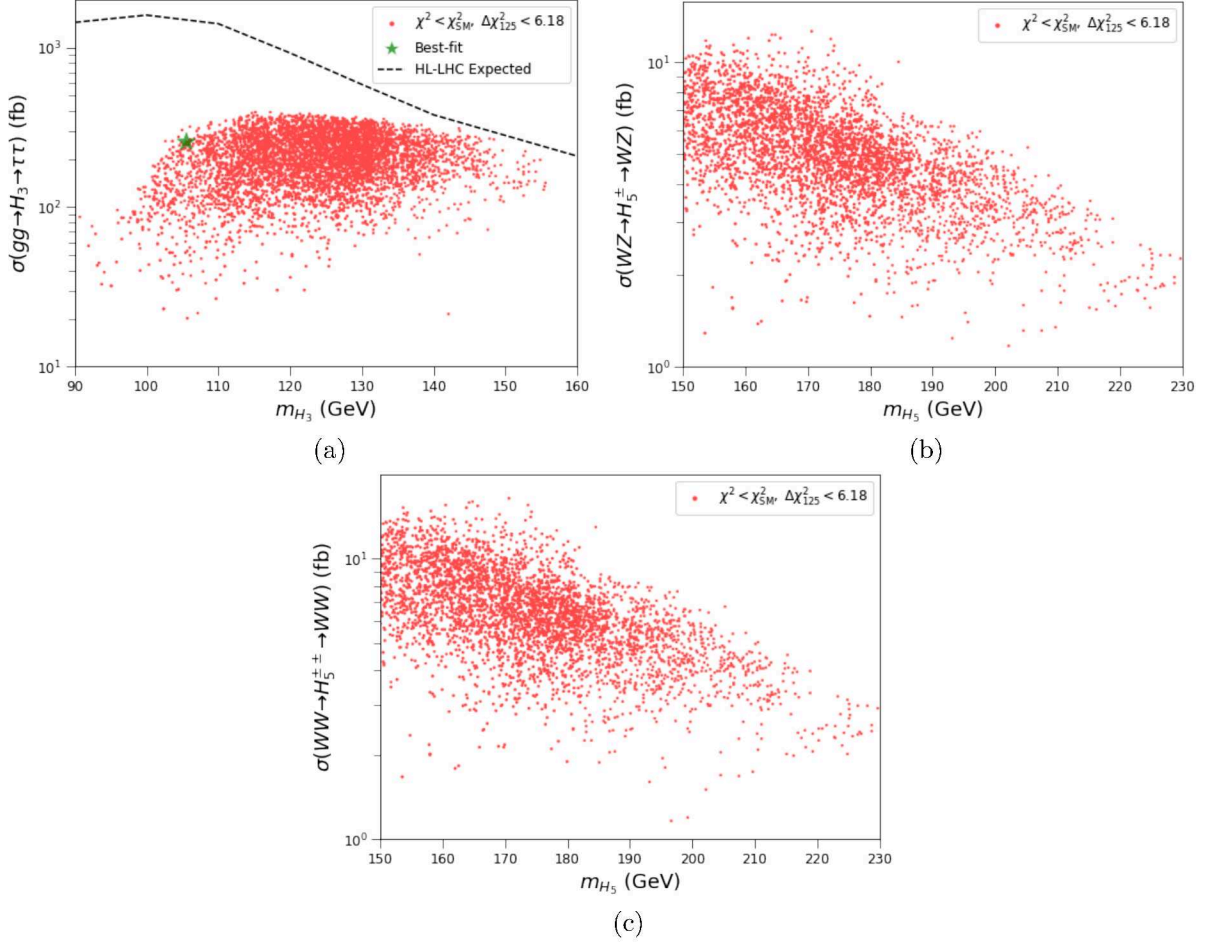


FIG. 4. Sample distributions in the (a)  $m_{H_3}$ - $\sigma(gg \rightarrow H_3 \rightarrow \tau\tau)$ , (b)  $m_{H_5}$ - $\sigma(WZ \rightarrow H_5^{\pm} \rightarrow WZ)$ , and (c)  $m_{H_5}$ - $\sigma(WW \rightarrow H_5^{\pm\pm} \rightarrow WW)$  planes at the 14-TeV LHC for case (i). In (a) we further show the expected 95% CL HL-LHC exclusion bound [105].

mass below 200 GeV can be probed at the LHC. Recently, a new method was presented, targeting this doubly-charged Higgs-boson mass scale [113]. The new search strategy focuses on  $H^{\pm\pm}$  pair production in the highly boosted regime, i.e., on  $H^{++}H^{--}$  pairs with large  $p_T$ , with one of them decaying via a pair of same-sign  $W$  bosons to a fat jet and the other decaying via another pair of same-sign  $W$  bosons to two adjacent same-sign leptons and two neutrinos, i.e.,  $p_T^{\text{miss}}$ . While the requirement of large  $p_T$  results in a significant reduction of the number of signal events, the SM background is even further suppressed, particularly via a discrimination of the fat jet from SM background jets. Depending on the mass of the doubly-charged Higgs boson, Ref. [113] claims to have sensitivity to discover doubly-charged Higgs bosons with less than  $\sim 160 \text{ fb}^{-1}$  of LHC data, in the mass range between 100 GeV and 200 GeV. While no such search, employing all the currently available data, has been performed so far, this indicates that the GM model interpretation of the

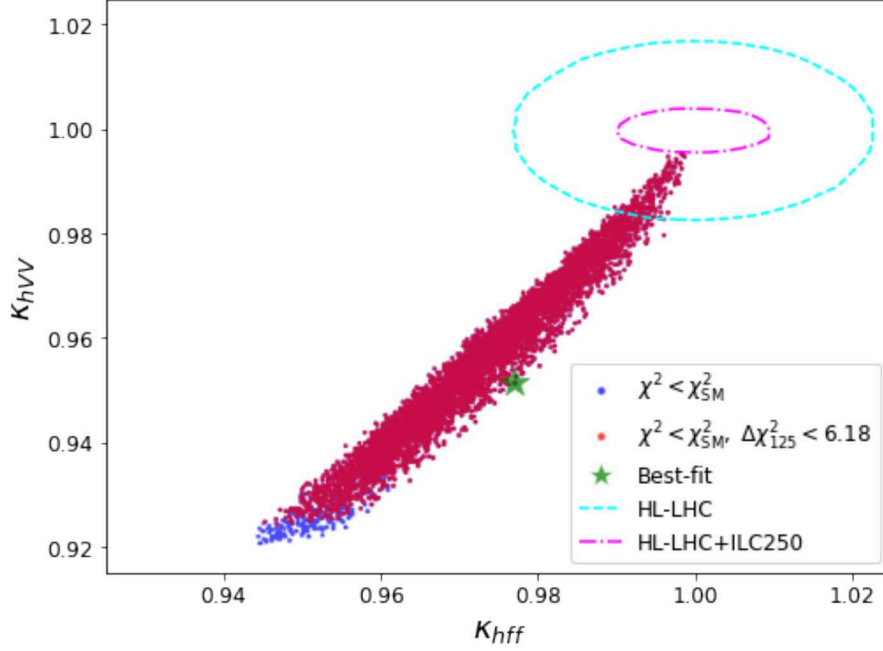


FIG. 5. Sample distribution in the  $\kappa_{hff}$ - $\kappa_{hVV}$  plane for case (i) and the prospective precision at the  $1\sigma$  level (indicated for the SM value) at the HL-LHC (cyan) [105] and the HL-LHC+ILC250 (magenta) [106].

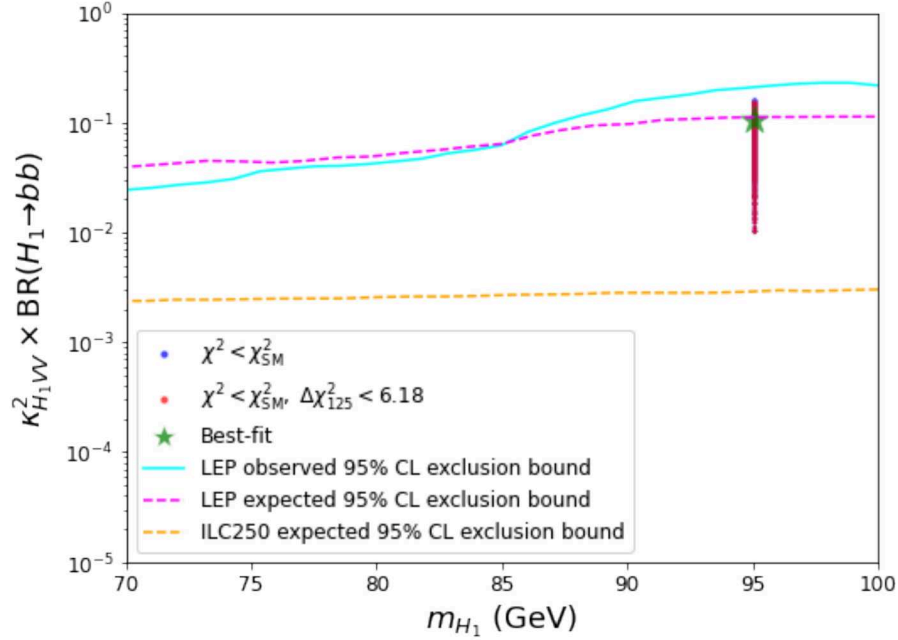


FIG. 6. Sample distribution in the  $m_{H_1}$ - $\kappa_{hVV}^2 \times \text{BR}(H_1 \rightarrow bb)$  plane for case (i) and the 95% CL LEP observed exclusion bound [6] (cyan), the 95% CL LEP expected exclusion bound [6] (magenta), and a projection for the 95% CL ILC250 expected exclusion bound [107] (orange).

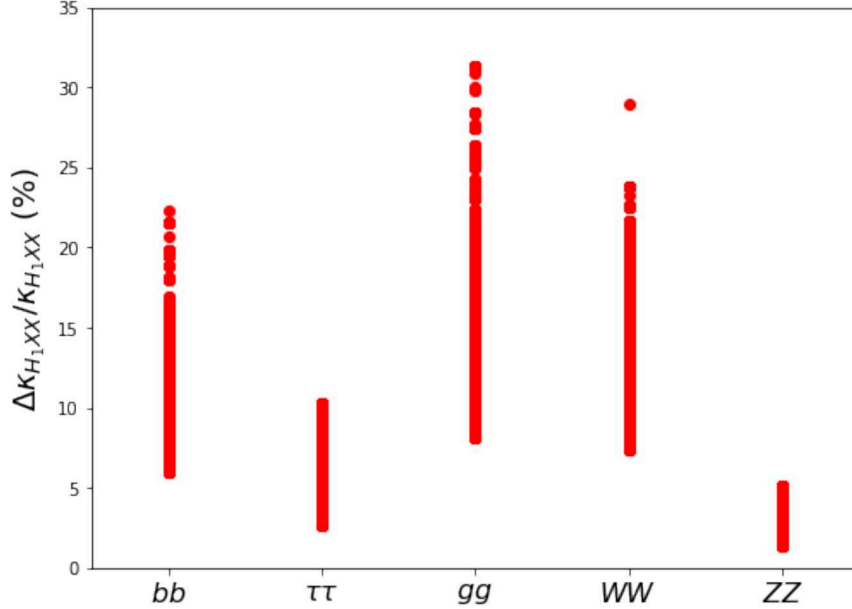


FIG. 7. Sample distributions for case (i) of  $\Delta\kappa_{H_1,XX}/\kappa_{H_1,XX}$ ,  $XX = bb, \tau\tau, gg, WW, ZZ$ .

excesses around  $\sim 95$  GeV may be testable in the upcoming LHC Runs.

Finally, we analyze the potential of future  $e^+e^-$  colliders to further probe the GM interpretation of the 95 GeV excesses. We first present in FIG. 5 the sample distribution in the  $\kappa_{hff} - \kappa_{hVV}$  plane overlaid with the anticipated precisions for the coupling measurements at the HL-LHC (cyan dashed) [105] and combined with (hypothetical future) ILC250 measurements (magenta dot-dashed) [106]. The ellipses in the plot are centered around the SM prediction of  $\kappa_{hff} = \kappa_{hVV} = 1$ . The deviations predicted in the  $h$  couplings w.r.t. the SM predictions can be very small (see the discussion above). Consequently, a sizable fraction of the sample points are within the  $1\sigma$  HL-LHC ellipse, and only the largest deviations would yield a  $\geq 3\sigma$  distinction of the GM and the SM. The situation is substantially improved for the case where the prospective ILC250 measurements are included. However, even including the  $e^+e^-$  coupling measurement a relevant part of the predicted points lies within  $2\sigma$  of the SM prediction. In the final step, we analyze the capabilities of the ILC to produce the new Higgs boson at  $\sim 95$  GeV, i.e.  $H_1$ , and to measure its couplings. In FIG. 6 we show the plane  $m_{H_1} - \kappa_{H_1} \times \text{BR}(H_1 \rightarrow b\bar{b})$ . The cyan (magenta) line indicates the observed (expected) exclusion obtained at LEP [6], where the  $\sim 2\sigma$  excess around 95 – 98 GeV can be seen. The dashed orange line indicates the improvements that can be expected at the ILC250 with an integrated luminosity of  $2 \text{ ab}^{-1}$  according to the projection of Ref. [107] (see also Ref. [114]). The blue points (which are a superset of the red points) show our selected sample, i.e. with  $\chi^2 < \chi_{\text{SM}}^2$ ,

where the red points furthermore fulfill  $\Delta\chi_{125}^2 < 6.18$ . It can clearly be observed that all parameter points within the preferred region are well within the projected ILC250 sensitivity. Consequently, it is expected within the GM model that the new Higgs boson at  $\sim 95$  GeV can be produced abundantly at the ILC250 (or other  $e^+e^-$  colliders operating at  $\sqrt{s} = 250$  GeV). In FIG. 7 we analyze the prospects of  $H_1$  coupling measurements at the ILC250. The evaluation of the anticipated precision of the coupling measurements is based on Ref. [40]. The evaluation has been performed for the (effective) couplings of the  $H_1$  to  $b\bar{b}$ ,  $\tau^+\tau^-$ ,  $gg$ ,  $WW$  and  $ZZ$ . While the first four rely on the decay of the Higgs boson to the respective final state, the  $H_1ZZ$  coupling is obtained from the production of the  $H_1$  as radiated from a  $Z$  boson. The latter channel yields the highest precision between 1 – 5%. A high accuracy is also expected for the coupling to  $\tau$ -leptons, ranging from 2 – 10%. The other three couplings are expected to be determined with an accuracy between  $\sim 6\%$  and  $\sim 30\%$ . Coupling measurements at this level of precision will help to distinguish the GM interpretation of the 95 GeV excesses from other model interpretations, see, e.g., Refs. [40, 41], where prospective coupling precisions for the N2HDM, 2HDMS and S2HDM have been evaluated.

## VI. CONCLUSIONS

If confirmed by further data, the excesses reported by CMS and ATLAS in the searches for low-mass Higgs bosons in the di-photon decay channel at a mass value of about 95 GeV could constitute a direct manifestation of an extended Higgs sector via the production of a new Higgs boson. In many previous model interpretations of the observed excesses in terms of a state  $\phi$ , extensions of the 2HDM were employed. This was mainly due to the possibility of a suppressed  $\phi b\bar{b}$  coupling, thereby enhancing  $\text{BR}(\phi \rightarrow \gamma\gamma)$  in such a way that the CMS and ATLAS excesses in this channel can be properly described. In the present paper, we have investigated a different possibility for enhancing the di-photon decay rate. Additional charged particles in the loop-mediated decay of a  $\sim 95$  GeV Higgs boson to two photons can yield a positive contribution to the decay rate and in this way result in a sufficiently strong rate. However, it was demonstrated in Ref. [24] that a second Higgs doublet, providing an additional singly-charged scalar, is not sufficient to yield a relevant effect on  $\text{BR}(\phi \rightarrow \gamma\gamma)$ .

The situation is different in BSM models that extend the Higgs sector with triplets. Such models predict the existence of doubly-charged Higgs bosons, which can substantially contribute to the di-photon decay rate of a new light, neutral Higgs boson that is also allowed to exist in the model. The GM model is of particular interest in this context, since despite containing Higgs triplets, it

preserves the electroweak  $\rho$ -parameter to be 1 at the tree level. We analyzed the di-photon excess within the GM model in conjunction with an excess in the  $b\bar{b}$  final state observed at LEP and an excess observed by CMS in the di-tau final state, which were found at comparable masses with local significances of about  $2\sigma$  and  $3\sigma$ , respectively. We demonstrated that within the GM model, a  $\sim 95$  GeV Higgs boson with a di-photon decay rate as observed by CMS and ATLAS can be well described. Simultaneously, the GM model can also accommodate the  $b\bar{b}$  excess at LEP, but not the di-tau excess. In this context, it is important to note that the signal strength observed by CMS in the  $gg \rightarrow \phi \rightarrow \tau^+\tau^-$  search is in some tension (depending on the model realization) with experimental bounds from recent searches performed by CMS for the production of a Higgs boson in association with a top-quark pair or in association with a  $Z$  boson, with subsequent decay into tau pairs, as well as with the searches performed at LEP for the process  $e^+e^- \rightarrow Z\phi(\phi \rightarrow \tau^+\tau^-)$ .

We have demonstrated in our analysis that the loop contribution of the doubly-charged Higgs boson indeed gives rise to an important upward shift in the di-photon rate of the Higgs boson at  $\sim 95$  GeV which is instrumental for bringing the predicted rate in agreement with the observed excesses. In the preferred parameter region, the doubly-charged Higgs boson is predicted to be rather light, with a mass in the range between 100 GeV and 200 GeV. While the LEP searches excluded doubly-charged Higgs bosons below  $\sim 100$  GeV using the di-tau final state, which is irrelevant to the preferred parameter space of this study, the searches that were conducted at the LHC so far only cover the mass region above  $\sim 200$  GeV.

Since also the other Higgs bosons of the GM model are predicted to be light in the considered scenario, a realization of the observed excesses at  $\sim 95$  GeV within the GM model would give rise to the exciting possibility that experimental confirmation of the excesses at  $\sim 95$  GeV could be accompanied by discoveries of further states of the extended Higgs sector. We have studied the prospects for probing the GM interpretation with results from future Runs of the LHC and from a future  $e^+e^-$  collider. While dedicated searches for low-mass doubly-charged Higgs bosons at the LHC could probe the preferred mass region, we find that the predicted rates for the production of Higgs bosons decaying to tau-pairs remain below the anticipated reach of the HL-LHC. A future  $e^+e^-$  collider would have good prospects for probing the GM interpretation of the observed excesses at  $\sim 95$  GeV via precision measurements of the couplings of the detected Higgs boson at about 125 GeV, via the direct search for the state at  $\sim 95$  GeV and via searches for the pair production of the doubly-charged Higgs boson of the GM model.

## ACKNOWLEDGMENTS

We thank S. Ashanujjaman and T. Biekötter for helpful discussions. C.W.C. is supported in part by the National Science and Technology Council of Taiwan under Grant No. NSTC-111-2112-M-002-018-MY3. The work of S.H. has received financial support from the grant PID2019-110058GB-C21 funded by MCIN/AEI/10.13039/501100011033 and by “ERDF A way of making Europe”, and in part by the grant IFT Centro de Excelencia Severo Ochoa CEX2020-001007-S funded by MCIN/AEI/10.13039/501100011033. S.H. also acknowledges support from Grant PID2022-142545NB-C21 funded by MCIN/AEI/10.13039/501100011033/ FEDER, UE. G.W. acknowledges support by the Deutsche Forschungsgemeinschaft (DFG, German Research Foundation) under Germany’s Excellence Strategy – EXC 2121 “Quantum Universe” – 390833306. This work has been partially funded by the Deutsche Forschungsgemeinschaft (DFG, German Research Foundation) - 491245950.

- 
- [1] G. Aad *et al.* (ATLAS), *Phys. Lett. B* **716**, 1 (2012), [arXiv:1207.7214 \[hep-ex\]](#).
  - [2] S. Chatrchyan *et al.* (CMS), *Phys. Lett. B* **716**, 30 (2012), [arXiv:1207.7235 \[hep-ex\]](#).
  - [3] A. Tumasyan *et al.* (CMS), *Nature* **607**, 60 (2022), [arXiv:2207.00043 \[hep-ex\]](#).
  - [4] G. Aad *et al.* (ATLAS), *Nature* **607**, 52 (2022), [Erratum: *Nature* 612, E24 (2022)], [arXiv:2207.00092 \[hep-ex\]](#).
  - [5] G. Abbiendi *et al.* (OPAL), *Eur. Phys. J. C* **27**, 311 (2003), [arXiv:hep-ex/0206022](#).
  - [6] R. Barate *et al.* (LEP Working Group for Higgs boson searches, ALEPH, DELPHI, L3, OPAL), *Phys. Lett. B* **565**, 61 (2003), [arXiv:hep-ex/0306033](#).
  - [7] S. Schael *et al.* (ALEPH, DELPHI, L3, OPAL, LEP Working Group for Higgs Boson Searches), *Eur. Phys. J. C* **47**, 547 (2006), [arXiv:hep-ex/0602042](#).
  - [8] (2012) [arXiv:1207.0449 \[hep-ex\]](#).
  - [9] *Search for new resonances in the diphoton final state in the mass range between 80 and 110 GeV in pp collisions at  $\sqrt{s} = 8$  TeV*, Tech. Rep. (CERN, Geneva, 2015).
  - [10] A. M. Sirunyan *et al.* (CMS), *Phys. Lett. B* **793**, 320 (2019), [arXiv:1811.08459 \[hep-ex\]](#).
  - [11] A. M. Sirunyan *et al.* (CMS), *JHEP* **09**, 007 (2018), [arXiv:1803.06553 \[hep-ex\]](#).
  - [12] *Search for resonances in the 65 to 110 GeV diphoton invariant mass range using 80 fb<sup>-1</sup> of pp collisions collected at  $\sqrt{s} = 13$  TeV with the ATLAS detector*, Tech. Rep. (CERN, Geneva, 2018).
  - [13] A. Tumasyan *et al.* (CMS), *JHEP* **07**, 073 (2023), [arXiv:2208.02717 \[hep-ex\]](#).
  - [14] G. Aad *et al.* (ATLAS), *JHEP* **07**, 155 (2023), [arXiv:2211.04172 \[hep-ex\]](#).

- [15] *Search for a standard model-like Higgs boson in the mass range between 70 and 110 GeV in the diphoton final state in proton-proton collisions at  $\sqrt{s} = 13$  TeV*, Tech. Rep. (CERN, Geneva, 2023).
- [16] J. Cao, X. Guo, Y. He, P. Wu, and Y. Zhang, *Phys. Rev. D* **95**, 116001 (2017), arXiv:1612.08522 [hep-ph].
- [17] P. J. Fox and N. Weiner, *JHEP* **08**, 025 (2018), arXiv:1710.07649 [hep-ph].
- [18] F. Richard, (2017), arXiv:1712.06410 [hep-ex].
- [19] U. Haisch and A. Malinauskas, *JHEP* **03**, 135 (2018), arXiv:1712.06599 [hep-ph].
- [20] T. Biekötter, S. Heinemeyer, and C. Muñoz, *Eur. Phys. J. C* **78**, 504 (2018), arXiv:1712.07475 [hep-ph].
- [21] F. Domingo, S. Heinemeyer, S. Paßehr, and G. Weiglein, *Eur. Phys. J. C* **78**, 942 (2018), arXiv:1807.06322 [hep-ph].
- [22] D. Liu, J. Liu, C. E. M. Wagner, and X.-P. Wang, *JHEP* **06**, 150 (2018), arXiv:1805.01476 [hep-ph].
- [23] J. M. Cline and T. Toma, *Phys. Rev. D* **100**, 035023 (2019), arXiv:1906.02175 [hep-ph].
- [24] T. Biekötter, M. Chakraborti, and S. Heinemeyer, *Eur. Phys. J. C* **80**, 2 (2020), arXiv:1903.11661 [hep-ph].
- [25] J. A. Aguilar-Saavedra and F. R. Joaquim, *Eur. Phys. J. C* **80**, 403 (2020), arXiv:2002.07697 [hep-ph].
- [26] T. Biekötter, S. Heinemeyer, and G. Weiglein, *Phys. Lett. B* **846**, 138217 (2023), arXiv:2303.12018 [hep-ph].
- [27] D. Azevedo, T. Biekötter, and P. M. Ferreira, *JHEP* **11**, 017 (2023), arXiv:2305.19716 [hep-ph].
- [28] T. Biekötter, in *57th Rencontres de Moriond on Electroweak Interactions and Unified Theories* (2023) arXiv:2304.11439 [hep-ph].
- [29] C. Arcangeletti (ATLAS), *LHC Seminar*, Tech. Rep. (2023).
- [30] *Search for diphoton resonances in the 66 to 110 GeV mass range using  $140 \text{ fb}^{-1}$  of 13 TeV pp collisions collected with the ATLAS detector*, Tech. Rep. (CERN, Geneva, 2023).
- [31] T. Biekötter, S. Heinemeyer, and G. Weiglein, (2023), arXiv:2306.03889 [hep-ph].
- [32] A. Azatov, R. Contino, and J. Galloway, *JHEP* **04**, 127 (2012), [Erratum: *JHEP* 04, 140 (2013)], arXiv:1202.3415 [hep-ph].
- [33] *Search for dilepton resonances from decays of (pseudo)scalar bosons produced in association with a massive vector boson or top quark anti-top quark pair at  $\sqrt{s} = 13$  TeV*, Tech. Rep. (CERN, Geneva, 2022).
- [34] W. G. Hollik, S. Liebler, G. Moortgat-Pick, S. Paßehr, and G. Weiglein, *Eur. Phys. J. C* **79**, 75 (2019), arXiv:1809.07371 [hep-ph].
- [35] K. Choi, S. H. Im, K. S. Jeong, and C. B. Park, *Eur. Phys. J. C* **79**, 956 (2019), arXiv:1906.03389 [hep-ph].
- [36] T. Biekötter, S. Heinemeyer, and C. Muñoz, *Eur. Phys. J. C* **79**, 667 (2019), arXiv:1906.06173 [hep-ph].

- [37] J. Cao, X. Jia, Y. Yue, H. Zhou, and P. Zhu, *Phys. Rev. D* **101**, 055008 (2020), [arXiv:1908.07206 \[hep-ph\]](#).
- [38] T. Biekötter and M. O. Olea-Romacho, *JHEP* **10**, 215 (2021), [arXiv:2108.10864 \[hep-ph\]](#).
- [39] T. Biekötter, A. Grohsjean, S. Heinemeyer, C. Schwanenberger, and G. Weiglein, *Eur. Phys. J. C* **82**, 178 (2022), [arXiv:2109.01128 \[hep-ph\]](#).
- [40] S. Heinemeyer, C. Li, F. Lika, G. Moortgat-Pick, and S. Paasch, *Phys. Rev. D* **106**, 075003 (2022), [arXiv:2112.11958 \[hep-ph\]](#).
- [41] T. Biekötter, S. Heinemeyer, and G. Weiglein, *JHEP* **08**, 201 (2022), [arXiv:2203.13180 \[hep-ph\]](#).
- [42] T. Biekötter, S. Heinemeyer, and G. Weiglein, *Eur. Phys. J. C* **83**, 450 (2023), [arXiv:2204.05975 \[hep-ph\]](#).
- [43] S. Iguro, T. Kitahara, and Y. Omura, *Eur. Phys. J. C* **82**, 1053 (2022), [arXiv:2205.03187 \[hep-ph\]](#).
- [44] A. Kundu, A. Le Yaouanc, P. Mondal, and F. Richard, in *2022 ECFA Workshop on e+e- Higgs/EW/Top factories* (2022) [arXiv:2211.11723 \[hep-ph\]](#).
- [45] J. A. Aguilar-Saavedra, H. B. Câmara, F. R. Joaquim, and J. F. Seabra, *Phys. Rev. D* **108**, 075020 (2023), [arXiv:2307.03768 \[hep-ph\]](#).
- [46] A. Le Yaouanc and F. Richard, in *2nd ECFA Workshop on e+e- Higgs/EW/Top Factories* (2023) [arXiv:2308.12180 \[hep-ph\]](#).
- [47] J. Cao, X. Jia, J. Lian, and L. Meng, (2023), [arXiv:2310.08436 \[hep-ph\]](#).
- [48] H. Georgi and M. Machacek, *Nucl. Phys. B* **262**, 463 (1985).
- [49] M. S. Chanowitz and M. Golden, *Phys. Lett. B* **165**, 105 (1985).
- [50] A. Ahriche, (2023), [arXiv:2312.10484 \[hep-ph\]](#).
- [51] C. H. de Lima and H. E. Logan, *Phys. Rev. D* **106**, 115020 (2022), [arXiv:2209.08393 \[hep-ph\]](#).
- [52] C.-W. Chiang and K. Yagyu, *JHEP* **01**, 026 (2013), [arXiv:1211.2658 \[hep-ph\]](#).
- [53] A. Ahriche, *Phys. Rev. D* **107**, 015006 (2023), [arXiv:2212.11579 \[hep-ph\]](#).
- [54] K. Hartling, K. Kumar, and H. E. Logan, *Phys. Rev. D* **90**, 015007 (2014), [arXiv:1404.2640 \[hep-ph\]](#).
- [55] M. Aoki and S. Kanemura, *Phys. Rev. D* **77**, 095009 (2008), [Erratum: *Phys.Rev.D* 89, 059902 (2014)], [arXiv:0712.4053 \[hep-ph\]](#).
- [56] W. G. Hollik, G. Weiglein, and J. Wittbrodt, *JHEP* **03**, 109 (2019), [arXiv:1812.04644 \[hep-ph\]](#).
- [57] P. M. Ferreira, M. Mühlleitner, R. Santos, G. Weiglein, and J. Wittbrodt, *JHEP* **09**, 006 (2019), [arXiv:1905.10234 \[hep-ph\]](#).
- [58] T.-K. Chen, C.-W. Chiang, and K. Yagyu, *Phys. Rev. D* **106**, 055035 (2022), [arXiv:2204.12898 \[hep-ph\]](#).
- [59] S. Blasi, S. De Curtis, and K. Yagyu, *Phys. Rev. D* **96**, 015001 (2017), [arXiv:1704.08512 \[hep-ph\]](#).
- [60] B. Keeshan, H. E. Logan, and T. Pilkington, *Phys. Rev. D* **102**, 015001 (2020), [arXiv:1807.11511 \[hep-ph\]](#).
- [61] T.-K. Chen, C.-W. Chiang, and K. Yagyu, *JHEP* **06**, 069 (2023), [Erratum: *JHEP* 07, 169 (2023)], [arXiv:2303.09294 \[hep-ph\]](#).

- [62] T.-K. Chen, C.-W. Chiang, C.-T. Huang, and B.-Q. Lu, *Phys. Rev. D* **106**, 055019 (2022), [arXiv:2205.02064 \[hep-ph\]](#).
- [63] J. De Blas *et al.*, *Eur. Phys. J. C* **80**, 456 (2020), [arXiv:1910.14012 \[hep-ph\]](#).
- [64] H. Bahl, T. Biekötter, S. Heinemeyer, C. Li, S. Paasch, G. Weiglein, and J. Wittbrodt, *Comput. Phys. Commun.* **291**, 108803 (2023), [arXiv:2210.09332 \[hep-ph\]](#).
- [65] P. Bechtle, S. Heinemeyer, O. Stål, T. Stefaniak, and G. Weiglein, *Eur. Phys. J. C* **74**, 2711 (2014), [arXiv:1305.1933 \[hep-ph\]](#).
- [66] P. Bechtle, S. Heinemeyer, O. Stål, T. Stefaniak, and G. Weiglein, *JHEP* **11**, 039 (2014), [arXiv:1403.1582 \[hep-ph\]](#).
- [67] P. Bechtle, S. Heinemeyer, T. Klingl, T. Stefaniak, G. Weiglein, and J. Wittbrodt, *Eur. Phys. J. C* **81**, 145 (2021), [arXiv:2012.09197 \[hep-ph\]](#).
- [68] P. Bechtle, O. Brein, S. Heinemeyer, G. Weiglein, and K. E. Williams, *Comput. Phys. Commun.* **181**, 138 (2010), [arXiv:0811.4169 \[hep-ph\]](#).
- [69] P. Bechtle, O. Brein, S. Heinemeyer, G. Weiglein, and K. E. Williams, *Comput. Phys. Commun.* **182**, 2605 (2011), [arXiv:1102.1898 \[hep-ph\]](#).
- [70] P. Bechtle, O. Brein, S. Heinemeyer, O. Stål, T. Stefaniak, G. Weiglein, and K. E. Williams, *Eur. Phys. J. C* **74**, 2693 (2014), [arXiv:1311.0055 \[hep-ph\]](#).
- [71] P. Bechtle, D. Dercks, S. Heinemeyer, T. Klingl, T. Stefaniak, G. Weiglein, and J. Wittbrodt, *Eur. Phys. J. C* **80**, 1211 (2020), [arXiv:2006.06007 \[hep-ph\]](#).
- [72] R. L. Workman *et al.* (Particle Data Group), *PTEP* **2022**, 083C01 (2022).
- [73] K. Hartling, K. Kumar, and H. E. Logan, (2014), [arXiv:1412.7387 \[hep-ph\]](#).
- [74] G. Aad *et al.* (ATLAS, CMS), *JHEP* **08**, 045 (2016), [arXiv:1606.02266 \[hep-ex\]](#).
- [75] M. Aaboud *et al.* (ATLAS), *Phys. Lett. B* **789**, 508 (2019), [arXiv:1808.09054 \[hep-ex\]](#).
- [76] G. Aad *et al.* (ATLAS), *Phys. Lett. B* **798**, 134949 (2019), [arXiv:1903.10052 \[hep-ex\]](#).
- [77] A. M. Sirunyan *et al.* (CMS), *JHEP* **03**, 003 (2021), [arXiv:2007.01984 \[hep-ex\]](#).
- [78] G. Aad *et al.* (ATLAS), *Eur. Phys. J. C* **80**, 957 (2020), [Erratum: *Eur.Phys.J.C* 81, 29 (2021), Erratum: *Eur.Phys.J.C* 81, 398 (2021)], [arXiv:2004.03447 \[hep-ex\]](#).
- [79] A. M. Sirunyan *et al.* (CMS), *Eur. Phys. J. C* **81**, 488 (2021), [arXiv:2103.04956 \[hep-ex\]](#).
- [80] A. M. Sirunyan *et al.* (CMS), *Phys. Rev. Lett.* **121**, 121801 (2018), [arXiv:1808.08242 \[hep-ex\]](#).
- [81] G. Aad *et al.* (ATLAS), *Eur. Phys. J. C* **81**, 178 (2021), [arXiv:2007.02873 \[hep-ex\]](#).
- [82] G. Aad *et al.* (ATLAS), *Eur. Phys. J. C* **81**, 537 (2021), [arXiv:2011.08280 \[hep-ex\]](#).
- [83] G. Aad *et al.* (ATLAS), *JHEP* **06**, 097 (2022), [arXiv:2111.06712 \[hep-ex\]](#).
- [84] A. M. Sirunyan *et al.* (CMS), *JHEP* **03**, 131 (2020), [arXiv:1912.01662 \[hep-ex\]](#).
- [85] *Direct constraint on the Higgs-charm coupling from a search for Higgs boson decays to charm quarks with the ATLAS detector*, Tech. Rep. (CERN, Geneva, 2021).
- [86] M. Aaboud *et al.* (ATLAS), *Phys. Rev. D* **99**, 072001 (2019), [arXiv:1811.08856 \[hep-ex\]](#).

- [87] *Measurement of Higgs boson production and decay to the  $\tau\tau$  final state*, Tech. Rep. (CERN, Geneva, 2019).
- [88] A. Tumasyan *et al.* (CMS), *JHEP* **06**, 012 (2022), arXiv:2110.04836 [hep-ex].
- [89] A. Tumasyan *et al.* (CMS), *Eur. Phys. J. C* **83**, 562 (2023), arXiv:2204.12957 [hep-ex].
- [90] G. Aad *et al.* (ATLAS), *Phys. Lett. B* **812**, 135980 (2021), arXiv:2007.07830 [hep-ex].
- [91] A. M. Sirunyan *et al.* (CMS), *JHEP* **01**, 148 (2021), arXiv:2009.04363 [hep-ex].
- [92] *Measurement of the properties of Higgs boson production at  $\sqrt{s}=13$  TeV in the  $H \rightarrow \gamma\gamma$  channel using  $139 \text{ fb}^{-1}$  of pp collision data with the ATLAS experiment*, Tech. Rep. (CERN, Geneva, 2020).
- [93] A. M. Sirunyan *et al.* (CMS), *JHEP* **07**, 027 (2021), arXiv:2103.06956 [hep-ex].
- [94] G. Aad *et al.* (ATLAS), *JHEP* **07**, 088 (2023), arXiv:2207.00348 [hep-ex].
- [95] A. M. Sirunyan *et al.* (CMS), *JHEP* **08**, 066 (2018), arXiv:1803.05485 [hep-ex].
- [96] *Analysis of  $t\bar{t}H$  and  $t\bar{t}W$  production in multilepton final states with the ATLAS detector*, Tech. Rep. (CERN, Geneva, 2019).
- [97] A. M. Sirunyan *et al.* (CMS), *Eur. Phys. J. C* **81**, 378 (2021), arXiv:2011.03652 [hep-ex].
- [98] M. Magg and C. Wetterich, *Phys. Lett. B* **94**, 61 (1980).
- [99] T. P. Cheng and L.-F. Li, *Phys. Rev. D* **22**, 2860 (1980).
- [100] G. Lazarides, Q. Shafi, and C. Wetterich, *Nucl. Phys. B* **181**, 287 (1981).
- [101] R. N. Mohapatra and G. Senjanovic, *Phys. Rev. D* **23**, 165 (1981).
- [102] *Measurement and interpretation of same-sign W boson pair production in association with two jets in pp collisions at  $\sqrt{s} = 13$  TeV with the ATLAS detector*, Tech. Rep. (CERN, Geneva, 2023).
- [103] S. Heinemeyer, C. Mariotti, G. Passarino, R. Tanaka, *et al.* (LHC Higgs Cross Section Working Group), (2013), 10.5170/CERN-2013-004, arXiv:1307.1347 [hep-ph].
- [104] D. de Florian *et al.* (LHC Higgs Cross Section Working Group), **2/2017** (2016), 10.23731/CYRM-2017-002, arXiv:1610.07922 [hep-ph].
- [105] M. Cepeda *et al.*, *CERN Yellow Rep. Monogr.* **7**, 221 (2019), arXiv:1902.00134 [hep-ph].
- [106] P. Bambade *et al.*, (2019), arXiv:1903.01629 [hep-ex].
- [107] P. Drechsel, G. Moortgat-Pick, and G. Weiglein, *Eur. Phys. J. C* **80**, 922 (2020), arXiv:1801.09662 [hep-ph].
- [108] G. Abbiendi *et al.* (OPAL), *Phys. Lett. B* **526**, 221 (2002), arXiv:hep-ex/0111059.
- [109] A. M. Sirunyan *et al.* (CMS), *Phys. Rev. Lett.* **120**, 081801 (2018), arXiv:1709.05822 [hep-ex].
- [110] M. Aaboud *et al.* (ATLAS), *Eur. Phys. J. C* **79**, 58 (2019), arXiv:1808.01899 [hep-ex].
- [111] G. Aad *et al.* (ATLAS), *JHEP* **06**, 146 (2021), arXiv:2101.11961 [hep-ex].
- [112] A. M. Sirunyan *et al.* (CMS), *Eur. Phys. J. C* **81**, 723 (2021), arXiv:2104.04762 [hep-ex].
- [113] S. Ashanujjaman, K. Ghosh, and R. Sahu, *Phys. Rev. D* **107**, 015018 (2023), arXiv:2211.00632 [hep-ph].
- [114] Y. Wang, J. List, and M. Berggren, in *International Workshop on Future Linear Collider* (2018) arXiv:1801.08164 [hep-ex].